Biosensors and Bioelectronics 143 (2019) 111632

Contents lists available at ScienceDirect

Biosensors and Bioelectronics

journal homepage: www.elsevier.com/locate/bios

Sunlight based handheld smartphone spectrometer

Dan Jian[a,1], Bin Wang[b,1], Huachuan Huang[c], Xin Meng[a,2], Cheng Liu[d], Liang Xue[e], Fei Liu[b,**], Shouyu Wang[a,b,*]

[a] Computational Optics Laboratory, School of Science, Jiangnan University, Wuxi, Jiangsu, 214122, China
[b] Single Molecule Nanometry Laboratory (Sinmolab), Nanjing Agricultural University, Nanjing, 210095, China
[c] School of Manufacturing Science and Engineering, Southwest University of Science and Technology, Mianyang, Sichuan, 621010, China
[d] Shanghai Institute of Optics and Fine Mechanics, Chinese Academy of Sciences, Shanghai, 201800, China
[e] College of Electronics and Information Engineering, Shanghai University of Electric Power, Shanghai, 200090, China

ARTICLE INFO

Keywords:
Handheld smartphone spectrometer
Sunlight source
On-site detection
Point-of-care testing
Virus detection

ABSTRACT

We present a sunlight based handheld smartphone spectrometer. The device first gathers the sunlight to pass through the sample, and then the transmitted light illuminates on a grating to generate spectrum finally recorded by the smartphone monochrome camera. All the optical elements are assembled with the smartphone to integrate a handheld device with the size of 140.2 mm × 67.4 mm × 80.5 mm. Besides, a smartphone application is also developed for automatic spectral calibration, detection, analysis and display. Compared to the white light emitting diode and the halogen lamp, the sunlight has more uniform distribution covering the entire visible spectral range; and the proposed device also avoids the bulky sizes of those broadband light sources. Additionally, the monochrome camera is used instead of the color camera not only to pursue a high spectral resolution as 0.276 nm/pixel but also to avoid the color overlapping. We demonstrate the device capability on detecting avian influenza virus H7N9 and porcine circovirus type 2 antibodies, proving the device has rather high sensitivity similar to the commercial microplate reader. Considering its advantages as compact size, high spectral resolution and detecting sensitivity, it is believed the proposed sunlight based handheld smartphone spectrometer is potential to be broadly applied in on-site detections.

1. Introduction

Optical spectroscopy focusing on spectral measurements and analysis is a powerful tool in various researches and applications, such as biological detections (Cialla-May et al., 2017; Manley, 2014), medical diagnostics (Haas and Mizaikoff, 2016) and food assessments (Ellis et al., 2012; Rodriguez-Saona and Allendorf, 2011), etc. Though commercial spectrometers utilized in the industries and laboratories can measure the spectra in high accuracy and resolution, they are often bulky and complicated; besides, most of them require external power supply, limiting their on-site applications. In order to extend their application scope, portable spectrometers have been designed and used in various applications (Al-Qazwini et al., 2016; Liu et al., 2018). Additionally, miniature systems such as micro-spectrometers based on advanced micro-opto-electro-mechanical systems (Hamamatsu Photonics) and ultra-mobile spectrometers relying on digital micro-mirror devices (Texas Instruments) have also been proposed to further compact the spectrometers. Unfortunately, most of them cannot support standalone operations, since they still require extra computers for data processing and display. Besides, both these bulky and compact spectrometers are often expensive, inevitably impeding their extensive applications.

Considering the smartphones not only have high-quality cameras for optical signal recording, but also have powerful processors for data processing and display, different smartphone based devices have been designed, such as smartphone microscopes for cell and tissue imaging (Breslauer et al., 2009; Cho et al., 2016; Ghassemi et al., 2017; Kühnemund et al., 2017; Meng et al., 2017; Shan et al., 2019; Shrivastava et al., 2018; Skandarajah et al., 2014; Switz et al., 2014; Wei et al., 2013, 2014a), smartphone sensors for biological and chemical detections (Berg et al., 2015; Choi., 2019; Kong et al., 2017; Lee et al., 2014; Li et al., 2017, 2019; Nguyen et al., 2018; Rajendran et al.,

* Corresponding author. Computational Optics Laboratory, School of Science, Jiangnan University, Wuxi, Jiangsu, 214122, China.
** Corresponding author.
E-mail addresses: feiliu24@njau.edu.cn (F. Liu), shouyu@jiangnan.edu.cn (S. Wang).
[1] These authors contributed equally to this work.
[2] Present Address: Department of Imaging Physics, Delft University of Technology, Delft, 2628 CJ, the Netherlands

https://doi.org/10.1016/j.bios.2019.111632
Received 15 June 2019; Received in revised form 10 August 2019; Accepted 23 August 2019
Available online 28 August 2019
0956-5663/

2019; Wei et al., 2014b) and smartphone spectrometers for spectral measurements and analysis (Long et al., 2014, 2017; Wang et al., 2016, 2018; Zhang et al., 2016). Long et al. (2014) proposed a smartphone spectrometer for both disease biomarker and food allergen detection using enzyme linked immunosorbent assays (ELISA); besides, they also reported multimode smartphone spectrometer which measured the spectra in both transmission and reflection modes (Long et al., 2017). Zhang et al. (2016) introduced an ultra-thin Fresnel lens combining the functions of collimation, dispersion and collection into the smartphone spectrometer to further compact its configuration. Wang et al. (2016) used digital versatile disc (DVD) instead of grating to build an ultra-low-cost smartphone spectrometer; moreover, they also proposed an octochannel smartphone spectrometer for mobile health diagnostics (Wang et al., 2018). Compared to those commercial spectrometers, these portable and affordable smartphone spectrometers can support their standalone operations such as spectral signal recording, data processing and display, completely avoiding external power supply and extra computer, suggesting that these smartphone spectrometers are especially suited for on-site applications. But note that most of these smartphone spectrometers use color CMOS cameras for spectrum recording, Bayer color filter array in color CMOS sensors inevitably decreases the resolution and the efficiency since four pixels are treated as a "new" pixel to show both amplitude and color; and the color filters in Bayer color filter array reduce the light intensity (Dubois, 2005; Jee et al., 2018; Pei and Tam, 2003). In addition, Bayer color filter array also induces color overlapping with large tilting illuminations thus decreasing the accuracy in spectral measurements (Dong et al., 2014; Fang et al., 2017). Moreover, some of these smartphone spectrometers used white light emitting diode (LED) as the light source (Wang et al., 2016, 2018), unfortunately, its spectrum is not evenly distributed in the visible light range (Cho et al., 2017). Though broadband light sources such as halogen lamps can provide more evenly distributed spectrum, they can hardly be integrated in the handheld smartphone spectrometers due to their sizeable configuration.

In this paper, we design a sunlight based handheld smartphone spectrometer. It uses sunlight as the illumination source, which spectrum is more uniformly distributed in visible light band compared to those of the white LED and the halogen lamp, and avoids the sizeable configuration of the often used broadband light sources. Besides, the smartphone monochrome CMOS camera is used for spectral signal recording, increasing the resolution and the efficiency as well as avoiding the color overlapping. In this design, only low-cost grating and lens are required and assembled with smartphone using 3-D printing fabricated structures, making the system compact with the size of only 140.2 mm × 67.4 mm × 80.5 mm. Additionally, a smartphone application is designed for rapid spectral calibration, detection, analysis and display. The proposed sunlight based handheld smartphone spectrometer can cover the entire visible light range from 380 nm to 760 nm with a high spectral resolution of 0.276 nm/pixel. Besides, the linear relation between the absorbance of standard Rhodamine 6G (R6G) and its concentration indicates the rather high accuracy of this proposed handheld smartphone spectrometer. We also present its capability on detecting avian influenza virus (AIV) H7N9 and porcine circovirus type 2 (PCV2) antibodies. AIV poses a significant threat to the poultry industry worldwide, which has the potential to cross species barriers to trigger human pandemics such as human infections with H7N9 (Gao et al., 2013). PCV2 is an essential pathogen for porcine circovirus-associated diseases (PCVADs) and caused great economic loss in domestic and overseas pig breeding (Afghah et al., 2017; Palinski et al., 2017). Therefore, it is critical to construct an accurate and sensitive method to implement the early diagnosis for AIV and PCV2 antibodies to prevent and control the spread of these viruses. The results reveal that the sunlight based handheld smartphone spectrometer can detect the target in rather high sensitivity similar to the commercial microplate reader. Considering its advantages as compact configuration, effective cost, fast speed, high spectral resolution, sensitivity and accuracy, it is believed the proposed sunlight based handheld smartphone spectrometer is potential to be broadly used in on-site detections.

2. Materials and methods

2.1. Chemicals and reagents

Potassium chloride (KCl), potassium dihydrogen phosphate (KH_2PO_4), sodium chloride (NaCl), sodium carbonate (Na_2CO_3), sodium bicarbonate ($NaHCO_3$) and disodium hydrogen phosphate (Na_2HPO_4) purchased from Sinopharm (China) were of analytical grade and used without further purification. Tween-20 was purchased from Sinopharm (China). Phosphate buffered saline (PBS, pH = 7.2) contained 137 mM NaCl, 2.7 mM KCl, 10 mM Na_2HPO_4 and 2 mM KH_2PO_4; and PBST is PBS with 1% Tween-20. Carbonate buffer solution (CBS, pH = 9.6) contained 15 mM Na_2CO_3 and 35 mM $NaHCO_3$. TMB color reagent A solution (3,3′,5,5′-tetramethylbenzidine solution) and TMB color reagent B solution (peroxide solution) were purchased from Aladdin (China). Bovine serum albumin (BSA) was purchased from Thermo Fisher (US). HRP-conjugated goat anti-mouse IgG antibody (HAb1) and HRP-conjugated goat anti-rabbit IgG antibody (HAb2) were purchased from Kirkegaard & Perry Laboratories (US). The simulated positive and negative serum of AIV H7N9 and PCV2, the AIV H7N9 monoclonal antibody and the PCV2 polyclonal antibody were prepared in our laboratory. Ultrapure water obtained from the Milli-Q system (Millipore, 18.2 MU resistivity, US) was used in experiments.

2.2. Sample preparation

In AIV H7N9 sample preparation, first, microtiter plates were coated with prokaryotic recombinant hemagglutinin protein (HA1) overnight at 4 °C with 100 μL/well at a concentration of 2 μg/mL in CBS. After washing three times with PBST, the plates were blocked with 5% BSA in PBS at 37 °C for 1 h with 200 μL/well. The plates were washed and air dried. Then, plates were incubated with different dilution ratios of AIV H7N9 antibody (10^3, 5×10^3, 10^4, 5×10^4, 10^5, 3×10^5, 5×10^5, 8×10^5, 10^6 times diluted in 0.01 M PBS) at 37 °C for 30 min. Positive and negative serum of H7N9 (1:1000) were added as positive and negative control. The plates were washed three times with PBST and incubated with HAb1 (1:5000) for 30 min at 37 °C. After the plates were washed three times, TMB color reagent A and B solutions were mixed and transferred to each well with 100 μL. With incubation at room temperature for 10 min, the reaction was stopped by 2M H_2SO_4. Finally, the samples in microtiter plates were first tested by the commercial microplate reader (Tecan, Switzerland) directly and then detected by the proposed sunlight based handheld smartphone spectrometer by transferring the sample solutions from microtiter plates to the cuvettes. The protocol for PCV2 sample preparation was the same as that of AIV sample preparation, except that the PCV2 antibody was diluted by 400, 800, 1600, 3200, 6400, 12800, 25600 and 51200 times in 0.01 M PBS.

2.3. Hardware design of the sunlight based handheld smartphone spectrometer

Fig. 1(A) shows the optical design of the sunlight based handheld smartphone spectrometer. The sunlight first passes through the cuvette (Purshee Optical Elements Co., Ltd., China) filled with the sample under detection. Reflected by a mirror (Daheng Optics, China), the transmitted light is then focused onto a pinhole (Daheng Optics, China) with the diameter of 100 μm using a biconvex lens (Daheng Optics, China). Next, the light passing through the pinhole is collected using another biconvex lens (Daheng Optics, China) and dispersed using the reflective diffraction grating (Thorlabs, US) of 1200 grooves/mm. The angle between the light axis and the grating is 27° for the first-order diffraction light collection. It is known that there is no dispersion in the zeroth-order diffraction (Hecht, 2016), indicating the spectrum cannot be

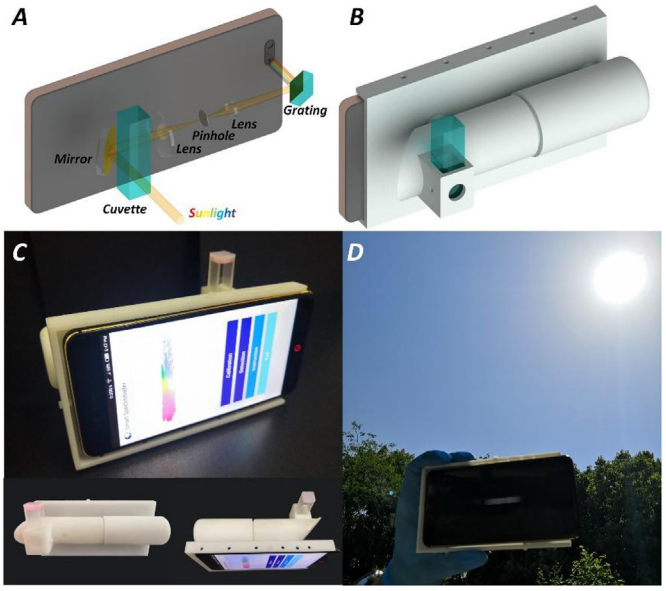

Fig. 1. Hardware design of the sunlight based handheld smartphone spectrometer. (A) optical design; (B) structure design; (C) constructed device; (D) device in application.

separated. Higher order diffractions can be used for spectral detection due to their dispersion capability, but the first-order diffraction has the highest intensity, which can maintain the high signal to noise ratio in measurements. Therefore, we collected the first-order diffraction for spectral detection. Finally, the monochrome CMOS sensor (IMX258, Sony, Japan) of the smartphone (Nubia, China) was used to collect the spectrum. The CMOS sensor has the size of 1/3.06″, the pixel size of 1.12 μm and the pixel number of 4224 × 3192. Moreover, in order to integrate the optical elements, the sample cuvette and the smartphone, 3-D printed structures were fabricated to construct the sunlight based handheld smartphone spectrometer as shown in Fig. 1(B). Fig. 1(C) shows the constructed device only with the size of 140.2 mm × 67.4 mm × 80.5 mm; moreover, no extra power supply is required. Fig. 1(D) shows its application in transmission spectra measurements.

2.4. Software design of the sunlight based handheld smartphone spectrometer

For automatic spectral calibration, detection, analysis and display, we develop an Android smartphone application called Smart Spectrometer as shown in Fig. 2. This application can deal with the spectral calibration, the wavelength-pixel relation retrieval and the spectral resolution evaluation. Fig. 2(A) is the application icon on the smartphone desktop, and Fig. 2(B) is the initial interface after starting this application. If there exists calibrated wavelength-pixel relation, spectral analysis can be directly implemented by clicking the "Detection" button in Fig. 2(B). Otherwise, spectral calibration should first be implemented to determine the wavelength-pixel relation by clicking the "Calibration" button in Fig. 2(B). Fig. 2(C) is the spectral calibration interface, in which the number of calibration wavelengths should be input, and note that more calibration wavelengths often obtain higher calibration accuracy, but require more lasers and spectral image captures. To balance the trade-off, here three wavelengths of 450 nm, 532 nm and 650 nm from laser diodes are used for spectral calibration. In Fig. 2(D), the first captured spectral image corresponding to 450 nm is read-in, and in Fig. 2(E), its corresponding wavelength is typed-in. Similarly, another two captured spectral images and their corresponding wavelengths as 532 nm and 650 nm are also input as shown in Fig. 2(F)–2(I). After reading-in all the calibration spectra, the smartphone application automatically recognizes the spectral peaks, since their corresponding wavelengths are known in advance, the wavelength-pixel relation can be precisely determined using linear fitting based on the least square method as shown in Fig. 2(J). The obtained wavelength-pixel relation can be saved for further spectral analysis by clicking the "Save" button in Fig. 2(J). In spectral calibration, for a specific wavelength, multiple spectral images can be read-in, and their average peak position is used for wavelength-pixel relation extraction. Next, the spectrum could be extracted from the captured spectral images according to the calibrated wavelength-pixel relation by clicking the "Detection" button in Fig. 2(B) or 2(J). The captured spectral image under analysis is read-in as shown in Fig. 2(K). Click the "Analysis" button, the spectral information could be finally displayed as shown in Fig. 2(L). It is worth noting that the displayed spectrum is not the intensity along a single pixel line, each point in the spectrum is the average intensity of central 50 pixels that are vertical to the spectral direction in the captured spectral image. Moreover, this displayed spectrum can be exported in txt file for further analysis by clicking "Export Spectrum" button.

2.5. Data analysis method

With the exported spectra, the relation between the sample concentration and the absorbance can finally be extracted. For each sample, often 5 repeated measurements are implemented to reduce the error. Besides, the absorbance spectra of the deionized water are also measured as the background. The absorbance is computed using optical density as $OD = -\log_{10}(T_{sample}/T_{deionized\ water})$ by normalizing the transmittance of sample against that of the deionized water, in which T_{sample} and $T_{deionized\ water}$ are the average transmittance of the sample and the deionized water at a specific wavelength from multiple measurements.

3. Results

3.1. Spectral calibration, spectral resolution and range evaluation

Three laser diodes (Haoran Optics, China) with the wavelengths of 450 nm, 532 nm and 650 nm were first used for spectral calibration. Fig. 3(A) lists the spectra extracted from the captured spectral images in the inserted image corresponding to different lasers, and their peaks were recognized to determine the pixels corresponding to these wavelengths. In order to extract the wavelength-pixel relation in high accuracy, 5 spectral images were first captured for each laser, then their corresponding spectral peaks were recognized, and finally their average value was used for linear fitting. Additionally, according to the grating principle (Hecht, 2016), the dispersion is linearly proportional to the wavelength, which means the pixel is linearly proportional to the wavelength. With this prior knowledge, the wavelength-pixel relation covering the entire visible light band can be linearly fitted using three lasers representing RGB wavelengths (Chang et al., 2018; Wang et al., 2018). Afterwards, the wavelength-pixel relation was determined via linear fitting as shown in Fig. 3(B), in which the coefficient of determination (R^2) is rather high as 0.999, indicating that the wavelength is linearly related to the pixel. Based on the determined linear wavelength-pixel relation, there were 724 pixels between the pixels corresponding to the wavelengths of 450 nm and 650 nm. Therefore, the proposed sunlight based handheld smartphone spectrometer could reach a high spectral resolution evaluated as (650 nm–450 nm)/724 pixels = 0.276 nm/pixel. All the spectral calibration, the wavelength-pixel relation retrieval and the spectral resolution evaluations were implemented using our designed Android smartphone application following the procedures shown in Fig. 2(C)–2(J). This proposed sunlight based handheld smartphone spectrometer can only be used for spectral detection in the visible light band, because the monochrome CMOS sensor (Sony IMX 258 mono) in the smartphone can only collect the

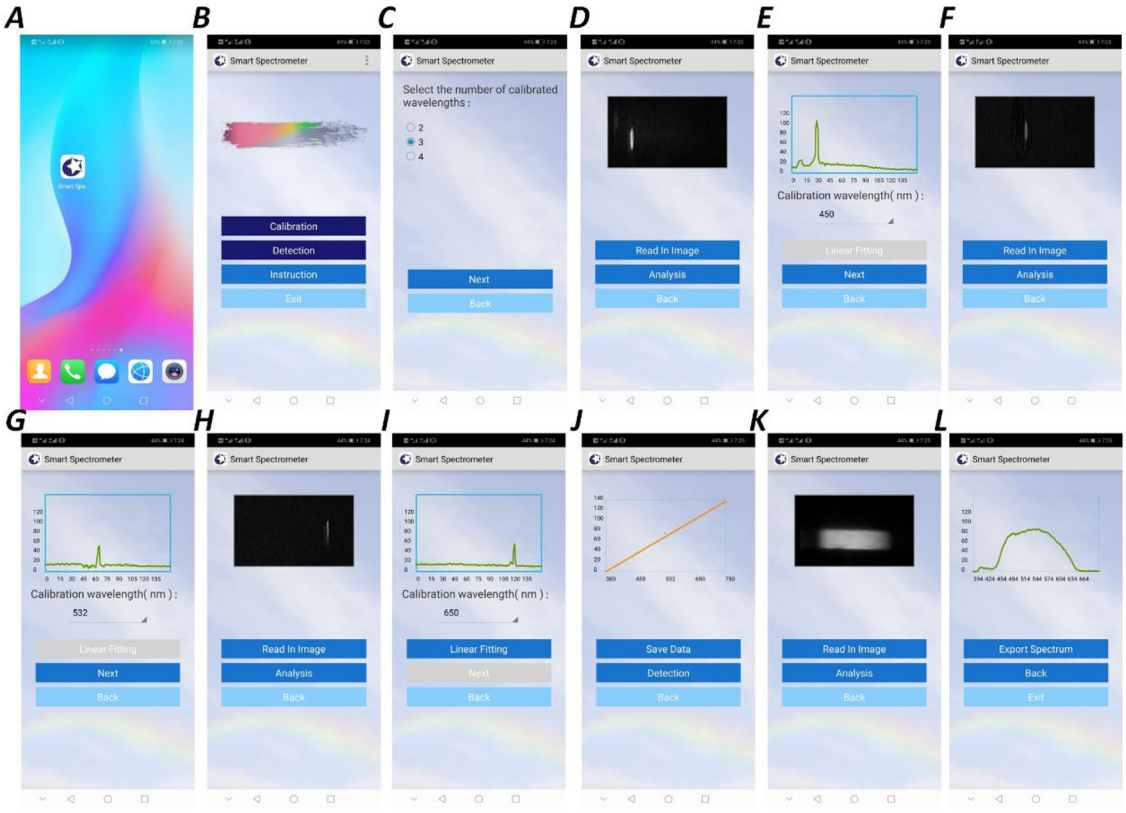

Fig. 2. Android application of the sunlight based handheld smartphone spectrometer. (A) application icon on the smartphone desktop; (B) initial interface; (C) calibration wavelength number selection; (D), (F) and (H) read-in the calibration spectral images; (E), (G) and (I) type-in the corresponding calibration wavelengths; (J) extract the wavelength-pixel relation; (K) read-in the spectral image for analysis; (L) display the spectrum.

visible light signals. In addition, with the linearly fitted wavelength-pixel relation, even the signals in the visible light band but beyond the range between 450 nm and 650 nm can still be accurately collected and recognized. In other words, for targets under detection, its corresponding spectra in visible light band can first be extracted from the captured spectral image, then the signals at specific wavelengths can be located, and finally the corresponding OD values can be computed according to the linearly fitted wavelength-pixel relation with high accuracy.

In order to test the accuracy of the proposed smartphone spectrometer, the spectra of the broadband light from a halogen lamp (Mshot, China) and a white LED (Daheng Optics, China) were measured using the proposed device and a commercial fiber spectrometer (IdeaOptics, China), and the results are listed in Fig. 3(C). The rather close spectral distributions prove that the handheld smartphone spectrometer not only can cover the visible light range from 380 nm to 760 nm, but also has rather high accuracy in spectral measurements. Additionally, Fig. 3(D) lists the spectra of the white LED, the halogen lamp and the sunlight measured by the proposed smartphone spectrometer. Compared to the spectra of the white LED and the halogen lamp, the sunlight spectrum is more uniformly distributed in the visible light band. When the signal under detection has the wavelength such as ~500 nm, the LED and halogen spectra can hardly maintain the high signal to noise ratio. While the sunlight spectrum is more evenly distributed in the visible band, thus our proposed device can easily maintain the high signal to noise ratio in the whole visible light band. Our designed device is more compact and simpler, since it did not require light source system as well as its power supply part. According to the spectral calibration as well as the spectral resolution and the range evaluation, the proposed sunlight based handheld smartphone spectrometer has the advantage as the linear wavelength-pixel relation, wide spectral range, high spectral resolution and accuracy in spectral measurements, therefore, it was then used in practical absorbance spectral measurements on R6G.

R6G as the standard sample was used to test the performance of proposed sunlight based handheld smartphone spectrometer. R6G was first diluted in the deionized water from 10 μg/mL to 2 μg/mL and then transferred to a series of cuvettes; besides, additional cuvettes filled with the deionized water were also prepared as the reference. Fig. 4(A) lists part of the captured spectral images and Fig. 4(B) lists their corresponding spectra in different R6G concentrations. According to the spectra in Fig. 4(B), though the spectral signals at 600 nm had higher values, they were not so sensitive to R6G concentrations, because the spectral signals at 600 nm did not change much in different R6G concentrations. According to the relation between the spectral absorption and the R6G concentration in Fig. 4(C), R6G had a concentration-dependent absorbance peak around the wavelength of 520 nm, and the OD520 value increased with higher R6G concentrations. Therefore, OD520 was used for R6G detection and further analysis. Additionally, the relation between OD520 and R6G concentration was linearly fitted as shown in Fig. 4(D) with the rather high coefficient of determination (R^2) of 0.997, proving the proposed sunlight based handheld smartphone spectrometer can be potentially used in quantitative target detection.

Moreover, the stability of the sunlight based handheld smartphone spectrometer was also tested. The sample was also R6G in deionized water solutions, and the OD520-concentration relations were extracted in various conditions. Fig. 4(E) shows the linearly fitted OD520-concentration relations measured on a sunny day but at different time as in the morning (tested from 9:00 to 10:00), at noon (tested from 12:30 to 13:30) and in the afternoon (tested from 15:00 to 16:00). Besides, Fig. 4(F) lists the linearly fitted OD520-concentration relations measured on a sunny day and a cloudy day. Moreover, the insert images in Fig. 4(E) and (F) are sunlight spectra without R6G measured by the

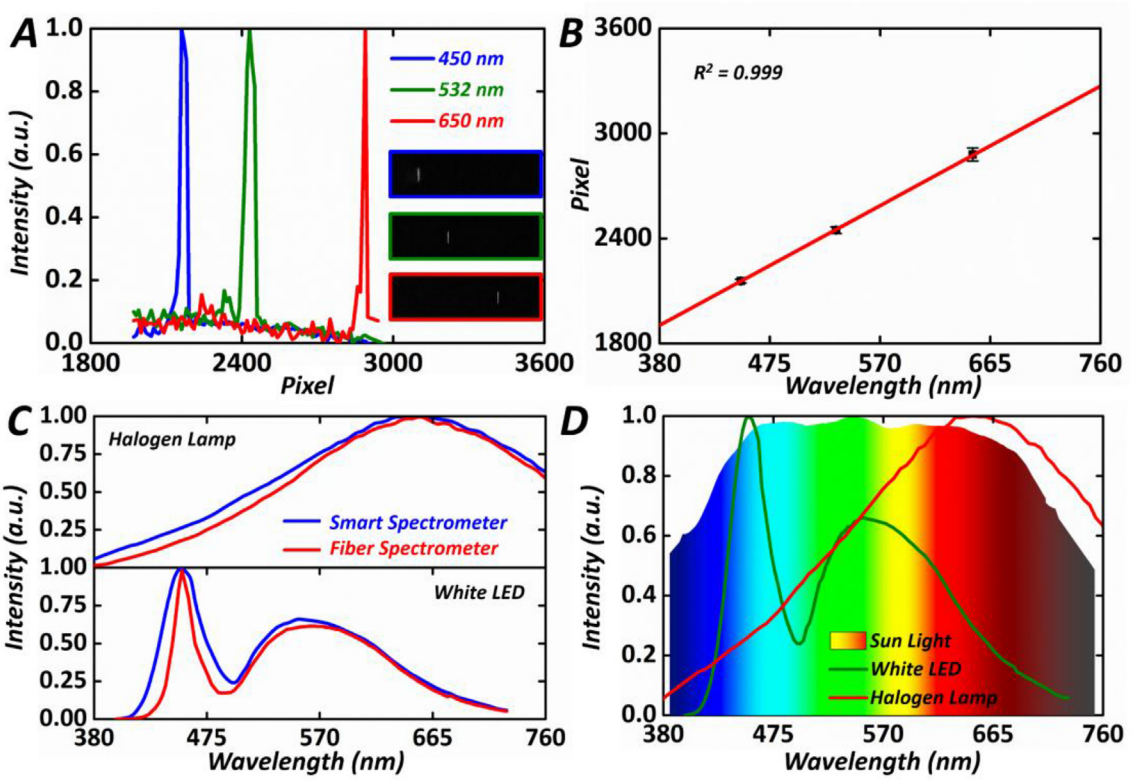

Fig. 3. Spectral calibration, spectral resolution and range evaluation. (A) spectra extracted from the captured spectral images corresponding to different lasers; (B) wavelength-pixel relation determined via linear fitting; (C) spectra of a halogen lamp and a white LED measured by the commercial fiber spectrometer and the proposed smartphone spectrometer; (D) spectra of the sunlight, the white LED and the halogen lamp measured by the proposed smartphone spectrometer. Verification on the Sunlight based Handheld Smartphone Spectrometer Using R6G.

sunlight based handheld smartphone spectrometer. Though there are differences in these sunlight spectra in various weather conditions, the OD520-concentration relations are still close with similar slopes with deviations less than 5%, proving that the sunlight based handheld smartphone spectrometer can provide stable results even measured at different time or weather.

According to the verification using R6G, it is proved that the proposed sunlight based handheld smartphone spectrometer can quantitatively detect the target; besides, it can also provide stable detections even measured at different time or weather.

3.2. Applications of the sunlight based handheld smartphone spectrometer on detecting AIV H7N9 and PCV2 antibodies

After the accuracy and stability verification on the sunlight based handheld smartphone spectrometer, the proposed device was finally adopted in AIV H7N9 and PCV2 antibody detections. HA1 is the main surface antigen of AIV, which can induce the production of protective neutralizing antibodies, and Cap protein is the main immune protective antigen for PCV2 inducing the immune response, therefore, HA1 and Cap protein based ELISA can be used for AIV H7N9 and PCV2 antibody detection. Samples with AIV H7N9 antibodies in different dilution ratios of 10^3, 5×10^3, 10^4, 5×10^4, 10^5, 3×10^5, 5×10^5 and PCV2 antibodies in different dilution ratios of 400, 800, 1600, 3200, 6400, 12,800, 25,600 as well as the negative serum as the reference were tested using the sunlight based handheld smartphone spectrometer, and 5 repeated measurements were implemented for each sample to reduce the error. Moreover, these measurements were all implemented in sunny days. Moreover, in order to test the accuracy of the proposed device, samples with AIV H7N9 and PCV2 antibodies in different dilution ratios as well as the negative serum were also tested using the commercial microplate reader (Tecan, Switzerland). Similarly, 5 repeated measurements were implemented for each sample to reduce the error. Fig. 5(A) and (B) compare the OD spectra of AIV H7N9 and PCV2 antibodies in specific dilution ratios measured from both the commercial and proposed devices.

In order to compare the accuracy of the proposed sunlight based handheld smartphone spectrometer, the discrete OD450 values in Fig. 5(C) and (D) were then extracted from Fig. 5(A) and (B), respectively. For the same dilution ratios, both OD450 values measured by the proposed and commercial devices are rather close. To quantitatively compare the results, the insert figure in Fig. 5(C) compares the OD450 values of the samples with AIV H7N9 antibodies in different dilution ratios of 10^3, 5×10^4 and 10^5, and that in Fig. 5(D) compares the OD450 values of the samples with PCV2 antibodies in different dilution ratios of 400, 6400 and 25600, representing the high, middle and low concentration cases. The OD450 data obtained by the commercial microplate reader and the proposed sunlight based handheld smartphone spectrometer are close in most conditions, proving the accuracy of the proposed sunlight based handheld smartphone spectrometer.

Moreover, for the proposed sunlight based handheld smartphone spectrometer, the detection limits on dilution ratios are 3×10^5 and 12800 for AIV H7N9 and PCV2 antibodies, respectively as shown in Fig. 4(C) and (D), since their measured OD450 values are all higher than that of the background plus 3 times standard deviation. Additionally, the detection limits were also proved by *t*-test, the *p* value between OD450 value of AIV H7N9 antibodies with dilution ratio of 3×10^5 or PCV2 antibodies with dilution ratio of 12800 and that of reference is lower than 0.05. While for the commercial microplate reader, the detection limits on dilution ratios are 8×10^5 and 25600 also as shown in Fig. 4(C) and (D) for AIV H7N9 and PCV2 antibodies, respectively. The detection limits were determined that the measurable OD450 values are all higher than that of the background plus 3 times standard deviation, besides, the detection limits were also verified by *t*-

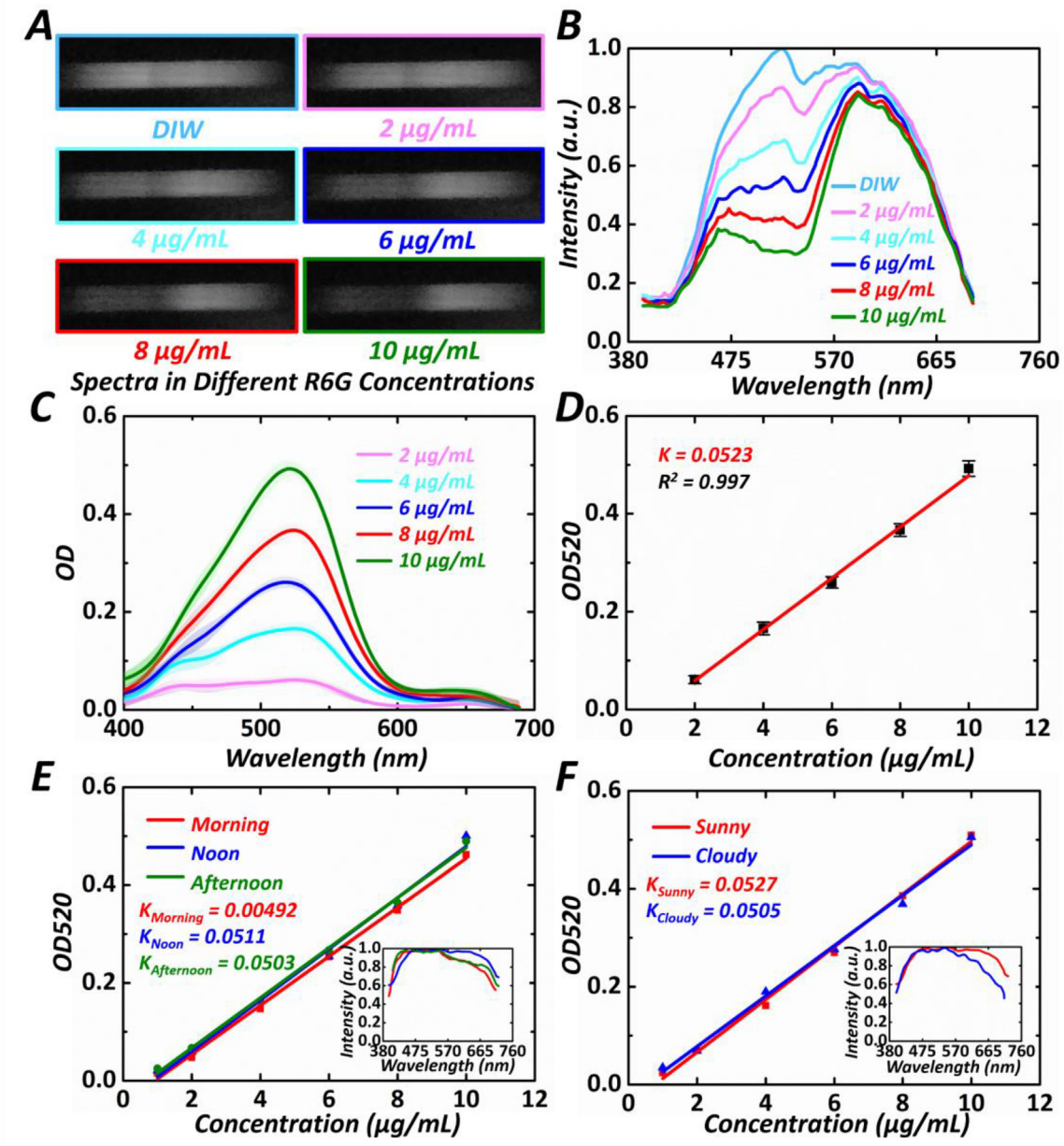

Fig. 4. Verification on the sunlight based handheld smartphone spectrometer using R6G. (A) captured spectral images; (B) spectra; (C) OD values and (D) OD520 values corresponding to different R6G concentrations; (E) linearly fitted OD520-concentration relations measured at different time on a sunny day; (F) linearly fitted OD520-concentration relations measured on a sunny day and a cloudy day; The insert images in (E) and (F) list the sunlight spectra in different conditions without R6G.

test. Though the sensitivity of the sunlight based handheld smartphone spectrometer is a little lower than that of the commercial microplate reader, the detection limit of the proposed device is still in the same order with that of the commercial one. Considering that the proposed device has much more compact configuration and cheaper cost, thus it is more suitable in on-site applications than the commercial microplate readers.

Finally, the upper bound of dilution ratio for AIV H7N9 antibody is 10^3, and that for PCV2 antibody is 400, since above the upper detection bounds, the absorbance at 450 nm is so strong (90% light intensity is absorbed) that the spectral signal to noise ratio is quite low, and it is difficult to distinguish the tiny spectral differences between two samples with both high concentrations. According to the upper detection bounds and the detection limits in both AIV H7N9 antibody and PCV2 antibody conditions, the effective detection ranges of the dilution ratios are 10^3-3×10^5 and 400–12800 for AIV H7N9 antibody and PCV2 antibody, respectively. In addition, the microplate reader had the effective detection ranges of dilution ratios of 10^3-8×10^5 and 400–25600 for AIV H7N9 antibody and PCV2 antibody, respectively. In Fig. 5(E) and (F), the linearly fitted relations between the logarithm of the dilution ratios and the OD450 values in effective detection ranges were computed. For the proposed sunlight based handheld smartphone spectrometer, the coefficients of determination (R^2) are 0.959 and 0.969 for AIV H7N9 and PCV2 antibody detections; and for the commercial microplate readers, the coefficients of determination (R^2) are 0.967 and 0.985. The high coefficients of determination suggest that the sunlight based handheld smartphone spectrometer can be potentially used for quantitative target detections.

Compared to spectrometer relying on the LED source, our designed device is more compact and simpler, since it did not require light source system or power supply part. Besides, LED spectrum is not evenly distributed in the visible light band as shown in Fig. 3(D). When the

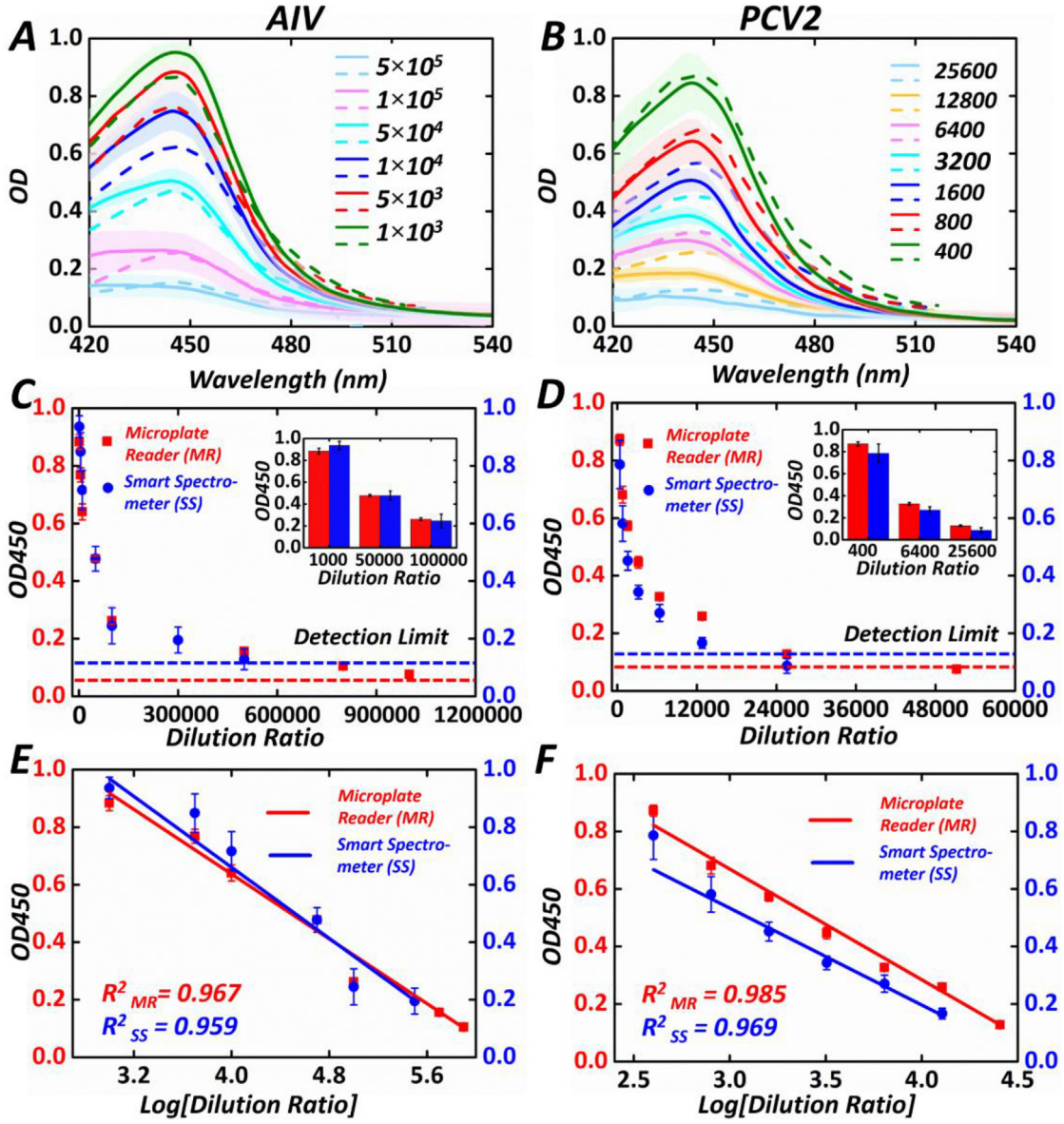

Fig. 5. Applications of the sunlight based handheld smartphone spectrometer on detecting AIV H7N9 and PCV2 antibodies. (A)/(B) OD values obtained from spectra measured by the proposed smartphone spectrometer (solid lines) and the commercial microplate reader (dashed lines) for AIV H7N9/PCV2 antibody in different dilution ratios. (C)/(D) OD450-dilution relations extracted from (A)/(B) for AIV H7N9/PCV2 cases. Insert figures: comparisons on OD450 obtained by the proposed and commercial devices in different dilution ratios. (E)/(F) Linearly fitted relation between OD450 values and the logarithm of dilution ratios for AIV H7N9/PCV2 cases.

signals under detection have some specific wavelengths such as ~500 nm, the LED spectrum can hardly maintain the high signal to noise ratio due to the rather low intensity at those wavelengths. While the sunlight spectrum is more evenly distributed in the visible light band also as shown in Fig. 3(D), which can easily maintain the high signal to noise ratio in spectral detection in the entire visible light band. Though the sensitivity of the sunlight based handheld smartphone spectrometer is a little lower than that of the commercial microplate reader, considering that the proposed device has much more compact configuration and cheaper cost, thus it is more suitable in on-site applications than the commercial microplate readers.

4. Conclusion

We present a sunlight based handheld smartphone spectrometer in this paper. It uses sunlight as the illumination source and avoids the bulky sizes of the traditionally used broadband light sources, therefore, it only has the small size of 140.2 mm × 67.4 mm × 80.5 mm. In addition, the sunlight spectrum is more evenly distributed in the visible light band than those of the white LED and the halogen lamp, which can easily maintain the high signal to noise ratio in spectral detection in the entire visible light band from 380 nm to 760 nm. Besides, instead of the color camera, the monochrome camera is used for spectral image recording not only to increase the spectral resolution and the light collection efficiency but also to avoid color overlapping. A smartphone application is developed for automatic spectral calibration and analysis in fast speed. The smartphone spectrometer can accurately detect the spectra covering the entire visible spectral range with the high spectral resolution of 0.276 nm/pixel. It was also successfully used in AIV H7N9 antibody and PCV2 antibody detection with high sensitivity and accuracy close to the commercial microplate reader. The sunlight based handheld smartphone spectrometer has the advantages as fast speed,

high spectral resolution, sensitivity and accuracy; moreover, it has rather compact configuration and does not rely on the external power supply, it is believed that the proposed device can be future used in medical and biological fields especially in on-site applications.

CRediT authorship contribution statement

Dan Jian: Data curation, Formal analysis, Investigation, Methodology, Software, Project administration, Validation, Visualization, Writing - original draft, Writing - review & editing. **Bin Wang:** Data curation, Formal analysis, Investigation, Methodology, Validation, Visualization, Writing - original draft, Writing - review & editing. **Huachuan Huang:** Investigation, Methodology, Visualization, Writing - review & editing. **Xin Meng:** Investigation, Methodology, Validation, Writing - original draft, Writing - review & editing. **Cheng Liu:** Formal analysis, Writing - review & editing. **Liang Xue:** Formal analysis, Writing - review & editing. **Fei Liu:** Funding acquisition, Investigation, Supervision, Validation, Writing - review & editing. **Shouyu Wang:** Conceptualization, Funding acquisition, Investigation, Supervision, Project administration, Validation, Writing - original draft, Writing - review & editing.

Declaration of competing interest

The authors declare the following financial interests/personal relationships which may be considered as potential competing interests: Fei Liu and Shouyu Wang are the co-founders of Sinmotec LLC, which commercializes the single molecule sensing and imaging techniques.

Acknowledgements

This work is supported by National Natural Science Foundation of China (61705092, 31870154, 31522056); Natural Science Foundation of Jiangsu Province of China (BK20170194); Jiangsu Key Research and Development Program (BE2018709).

References

Afghah, Z., Webb, B., Meng, X.J., Ramamoorthy, S., 2017. Vet. Microiol. 206, 21–28.
Al-Qazwini, Y., Noor, A.S.M., Al-Qazwini, Z., Yaacob, M.H., Harun, S.W., Mahdia, M.A., 2016. Sens. Actuators A Phys. 246, 163–169.
Berg, B., Cortazar, B., Tseng, D., Ozkan, H., Feng, S., Wei, Q., Chan, R.Y.L., Burbano, J., Farooqui, Q., Lewinski, M., Di Carlo, D., Garner, O.B., Ozcan, A., 2015. ACS Nano 9, 7857–7866.
Breslauer, D.N., Maamari, R.N., Switz, N.A., Lam, W.A., Fletcher, D.A., 2009. PLoS One 4, e6320.
Chang, Y.C., Ge, X., Wang, L.J., Lee, S.S., Paulsen, M.H., Khan, Q.M., Khalid, Z.M., Bhalli, J.A., Waheed, U., Simpson, C.D., Du, D., Li, L., Lin, Y., 2018. Sens. Actuators B Chem. 275, 300–305.
Cho, J., Park, J.H., Kim, J.K., Schubert, E.F., 2017. Laser Photonics Rev. 11, 1600147.
Cho, S., Islas-Robles, A., Nicolini, A.M., Monks, T.J., Yoon, J.Y., 2016. Biosens. Bioelectron. 86, 697–705.
Choi, W., Shin, J., Hyun, K.A., Song, J., Jung, H.I., 2019. Biosens. Bioelectron. 130, 414–419.
Cialla-May, D., Zheng, X.S., Weber, K., Popp, J., 2017. Chem. Soc. Rev. 46, 3945–3961.
Dong, S., Shiradkar, R., Nanda, P., Zheng, G., 2014. Biomed. Opt. Express 5, 1757–1767.
Dubois, E., 2005. IEEE Signal Process. Lett. 12, 847–850.
Ellis, D.I., Brewster, V.L., Dunn, W.B., Allwood, J.W., Golovanov, A.P., Goodacre, R., 2012. Chem. Soc. Rev. 41, 5706–5727.
Fang, J., Xu, H., Xu, P., Wang, Z., 2017. Optik 130, 50–60.
Gao, R., Cao, B., Hu, Y., Feng, Z., Wang, D., Hu, W., Chen, J., Jie, Z., Qiu, H., Xu, K., Xu, X., Lu, H., Zhu, W., Gao, Z., Xiang, N., Shen, Y., He, Z., Gu, Y., Zhang, Z., Yang, Y., Zhao, X., Zhou, L., Li, X., Zou, S., Zhang, Y., Li, X., Yang, L., Guo, J., Dong, J., Li, Q., Dong, L., Zhu, Y., Bai, T., Wang, S., Hao, P., Yang, W., Zhang, Y., Han, J., Yu, H., Li, D., Gao, G.F., Wu, G., Wang, Y., Yuan, Z., Shu, Y., 2013. N. Engl. J. Med. 368, 1888–1897.
Ghassemi, P., Wang, B., Wang, J., Wang, Q., Chen, Y., Pfefer, T.J., 2017. IEEE T. Bio. Med. Eng. 64, 1650–1653.
Haas, J., Mizaikoff, B., 2016. Annu. Rev. Anal. Chem. 9, 45–68.
Hamamatsu Photonics. https://www.hamamatsu.com/jp/en/product/optical-sensors/spectrometers/minispectrometer/index.html.
Hecht, E., 2016. Optics, fifth ed. Pearson, New Jersey.
Jee, S., Song, K.S., Kang, M.G., 2018. Sensors 18, 1647.
Kong, J.E., Wei, Q., Tseng, D., Zhang, J., Pan, E., Lewinski, M., Garner, O.B., Ozcan, A., Di Carlo, D., 2017. ACS Nano 11, 2934–2943.
Kühnemund, M., Wei, Q., Darai, E., Wang, Y., Hernandez-Neuta, I., Yang, Z., Tseng, D., Ahlford, A., Mathot, L., Sjoblom, T., Ozcan, A., Nilsson, M., 2017. Nat. Commun. 8, 13913.
Lee, S., Oncescu, V., Mancuso, M., Mehta, S., Erickson, D., 2014. Lab Chip 14, 1437–1442.
Li, J., Wang, X., Shan, Y., Huang, H., Jian, D., Xue, L., Wang, S., Liu, F., 2019. Micromachines 10, 27.
Li, X., Yang, F., Wong, J.X.H., Yu, H.Z., 2017. Anal. Chem. 89, 8908–8916.
Liu, T., Wang, W., Liu, F., Wang, S., 2018. Opt. Commun. 427, 301–305.
Long, K.D., Woodburn, E.V., Le, H.M., Shah, U.K., Lumetta, S.S., Cunningham, B.T., 2017. Lab Chip 17, 3246–3257.
Long, K.D., Yu, H., Cunningham, B.T., 2014. Biomed. Opt. Express 5, 3792–3806.
Manley, M., 2014. Chem. Soc. Rev. 43, 8200–8214.
Meng, X., Huang, H., Yan, K., Tian, X., Yu, W., Cui, H., Kong, Y., Xue, L., Liu, C., Wang, S., 2017. Lab Chip 17, 104–109.
Nguyen, H., Sung, Y., O'Shaughnessy, K., Shan, X., Shih, W., 2018. Anal. Chem. 90, 11517–11522.
Palinski, R., Piñeyro, P., Shang, P., Yuan, F., Guo, R., Fang, Y., Byers, E., Hause, B.M., 2017. J. Virol. 91 e01879-16.
Pei, S.C., Tam, I.K., 2003. IEEE T. Circ. Syst. Vid. 13, 503–513.
Rajendran, V.K., Bakthavathsalam, P., Bergquist, P.L., Sunna, A., 2019. Biosens. Bioelectron. 134, 68–75.
Rodriguez-Saona, L.E., Allendorf, M.E., 2011. Annu. Rev. Food Sci. T. 2, 467–483.
Shan, Y., Wang, B., Huang, H., Jian, D., Wu, X., Xue, L., Wang, S., Liu, F., 2019. Biosens. Bioelectron. 132, 238–247.
Skandarajah, A., Reber, C.D., Switz, N.A., Fletcher, D.A., 2014. PLoS One 9, e96906.
Shrivastava, S., Lee, W.I., Lee, N.E., 2018. Biosens. Bioelectron. 109, 90–97.
Switz, N.A., D'Ambrosio, M.V., Fletcher, D.A., 2014. PLoS One 9, e95330.
Texas Instruments. http://www.ti.com/tool/TIDA-00554?keyMatch=spectrometer&tisearch=Search-EN-Products.
Wang, L.J., Chang, Y.C., Ge, X., Osmanson, A.T., Du, D., Lin, Y., Li, L., 2016. ACS Sens. 1, 366–373.
Wang, L.J., Naudé, N., Chang, Y.C., Crivaro, A., Kamoun, M., Wang, P., Li, L., 2018. J. Biophot. 11, e201700382.
Wei, Q., Luo, W., Chiang, S., Kappel, T., Mejia, C., Tseng, D., Chan, R.Y.L., Yan, E., Qi, H., Shabbir, F., Ozkan, H., Feng, S., Ozcan, A., 2014a. ACS Nano 8, 12725–12733.
Wei, Q., Nagi, R., Sadeghi, K., Feng, S., Yan, E., Ki, S.J., Caire, R., Tseng, D., Ozcan, A., 2014b. ACS Nano 8, 1121–1129.
Wei, Q., Qi, H., Luo, W., Tseng, D., Ki, S.J., Wan, Z., Göröcs, Z., Bentolila, L.A., Wu, T.T., Sun, R., Ozcan, A., 2013. ACS Nano 7, 9147–9155.
Zhang, C., Cheng, G., Edwards, P., Zhou, M.D., Zheng, S., Liu, Z., 2016. Lab Chip 16, 246–250.